JOURNAL OF GUIDANCE, CONTROL, AND DYNAMICS
Vol. 15, No. 4, July-August 1992

Finite Element Approach for Transient Analysis of Multibody Systems

Shih-Chin Wu*
Lockheed Engineering and Sciences Company, Hampton, Virginia 23666
Che-Wei Chang*
COMTEK, Grafton, Virginia 23692
and
Jerrold M. Housner†
NASA Langley Research Center, Hampton, Virginia 23665

A three-dimensional, finite element based formulation for the transient dynamics of constrained multibody systems with trusslike configurations is presented. A convected coordinate system is used to define the rigid-body motion of individual elements in the system. Deformation of each element is defined relative to its convected coordinate system. The formulation is oriented toward joint-dominated structures. Through a series of sequential transformations, the joint degree of freedom is built into the equations of motion of the element to reduce geometric constraints. Based on the derivation, a general-purpose code has been developed. Two examples are presented to illustrate the application of the code.

Introduction

MANY recently proposed space structures are large and complex. To reduce packing volume, these structures may be delivered to orbit by the Space Shuttle and then deployed/assembled on orbit. To reduce weight, efficient designs of such systems tend to lead to flexible, low-frequency, and often joint-dominated structures. Consequently, interaction between rigid-body motion and structural deformation will likely occur. For efficient operation of structural systems requiring component articulation, it is desirable to maneuver components as rapidly as possible. However, operational speed is limited by excessive dynamic deformation if vibrations are not suppressed. In order to suppress excessive vibration responses, active controls may be utilized with the control design usually based on linear methods. This represents a significant design simplification since the articulation is governed by nonlinear equations. Moreover, another simplification is the use of reduced structural models. To assess the impact of these simplifications, analytical simulations are usually performed to examine design performance as well as stability.

Simulation codes for multibody systems such as DADS,[1] DISCOS,[2] and TREETOPS[3] use an assumed mode approach to describe the structural deformations of components. In other words, this approach requires users to select a set of deformation modes to represent flexibility for each flexible component. In general, deformation modes are obtained by solving an eigenvalue problem using general finite element programs. This requires that the question of what boundary conditions of the components shall be specified be answered. A flexible bar with pin joint at its ends may behave like a cantilever beam or simply supported beam, depending on the total equivalent mass and constraints at its ends. Note, also, that the equivalent masses and constraints are time varying. A second question requiring an answer is how many modes are needed and/or which modes shall be kept to represent flexibility for the components? The prediction of which modes will get excited in a flexible multibody system can be a difficult challenge since the system configurations are changing with time. It turns out that modal selection is often the most crucial part of the assumed mode approach. Since deformations of the component are defined as a linear combination of the selected modes, a component can only deform in the space spanned by the selected modes. Therefore, results of the modal approach will be in error if any inadequate modes are used in the simulation.

The purposes of this paper are to provide an alternative to the assumed mode approach that circumvents some of these difficulties and to describe the LATDYN (large angle transient dynamics) computer code used to implement this approach. The code is finite element based and models components using finite elements instead of a truncated set of modes, which would have to be generated outside the multibody analysis code. In order to separate the rigid-body motion and small deformations in the finite element approach, a coordinate system is chosen to represent the large displacement and rotation of each element. Deformations of each element are then defined with respect to the rigid-body configuration of the element. At the element level, mass matrices are calculated. The component mass matrix is obtained by assembing each elemental mass matrix as is typically done in conventional small motion/deformation finite element methods.

To form the system mass matrix, most multibody simulation codes impose nonlinear kinematic constraints on components that connect to the same joint. Instead of using constraint equations, the LATDYN program builds the hinge degree of freedom into the system equations of motion to connect components that share a common joint in a manner patterned after connectivity relations in conventional, small motion, finite elements. This approach ensures compatability between components. Since the mass of the interconnecting joint between the bodies represents a significant portion of the total mass the the orientation of the joint's hinge lines play an important role in determining structural behavior, it is thus reasonable to construct the finite element program with the joints as a part of element connectivity.

Kinematics of Beam Element

The kinematics developed here are applicable to arbitrarily large displacement and rotational motion of a beam with small

Received Oct. 31, 1990; revision received Aug. 2, 1991; accepted for publication Aug. 8, 1991.

*Research Scientist.

†Head, Computational Mechanics Branch.

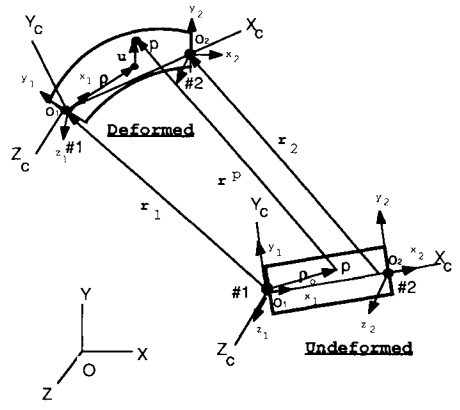

Fig. 1 Kinematics of beam element.

deformations. Consider the beam element with finite element nodes 1 and 2 at initial (undeformed) and current (deformed) configurations in an inertial $OXYZ$ frame, as shown in Fig. 1. To specify the configuration of the beam element, it is necessary to define a set of generalized coordinates that uniquely define the global displacement of every point in the deformed element. For each node of the element, an $o_i x_i y_i z_i$ $(i=1,2)$ nodal reference frame having its x axis tangent to the neutral axis of the beam and y and z axes coincide with the principle axes of the beam cross section is chosen to locate and orient the node in the inertial frame. Position vectors $\boldsymbol{r}_i$ $(i=1,2)$, from the origin of the initial $o_i x_i y_i z_i$ nodal reference frame to the origin of the current $o_i x_i y_i z_i$ nodal reference frame, define the global displacement of nodes 1 and 2. Transformation matrices $\boldsymbol{T}_i$, from nodal reference frames to the global frame, define orientations of the nodal reference frame. Deformation of the beam and displacement of any point in the beam now can be determined using $\boldsymbol{r}_i$ and $\boldsymbol{T}_i$.

Before deformations of the beam can be defined, rigid-body motion of the beam has to be separated from the total displacement of the beam. To specify rigid-body motion of the element, a convected coordinate system $o_1 X_c Y_c Z_c$ whose origin located at node 1 is used. Initially, the orientation of the convected coordinate system coincides with the nodal reference frame of both nodes 1 and 2. As the element moves with large displacement and small deformation, the orientation of the convected coordinate frame, hence, the rigid-body motion of the beam, is determined by defining the X_c axis of the $o_1 X_c Y_c Z_c$ frame to always lie along the line connecting nodes 1 and 2, and the Y_c axis to lie in the plane formed by the y axis of $o_1 x_1 y_1 z_1$ frame and the X_c axis of $o_1 X_c Y_c Z_c$ frame. With these definitions, the convected coordinate system is uniquely determined.

Deformations of the beam element are defined with respect to its rigid-body configuration as

$$\boldsymbol{D}_i = \boldsymbol{T}_c^T \boldsymbol{T}_i \tag{1}$$

where $\boldsymbol{T}_c$ denotes the transformation matrix from the rigid-body configuration (or the convected coordinate frame) to the global frame. Note that $\boldsymbol{D}_i$ can be regarded as a rotation about a vector from the undeformed state given by $\boldsymbol{T}_c$ to the current deformed state given by $\boldsymbol{T}_i$. Assuming that the rotation angles between $\boldsymbol{T}_i$ and $\boldsymbol{T}_c$ are small, then the components of this vector are the three rotation angles[4] measured with respect to the three axes of $\boldsymbol{T}_c$. Therefore, $\boldsymbol{D}_i$ can be simply represented by

$$\boldsymbol{D}_i = \begin{bmatrix} 1 & -\phi_{zi} & \phi_{yi} \\ \phi_{zi} & 1 & -\phi_{xi} \\ -\phi_{yi} & \phi_{xi} & 1 \end{bmatrix}$$

where ϕ_{xi}, ϕ_{yi}, and ϕ_{zi} are the rotation angles of $\boldsymbol{T}_i$ about the x, y, and z axes of the convected frame, respectively. Physically, they correspond to flexural deformations of the beam element at nodes 1 and 2.

The rotation angles may be readily extracted from $\boldsymbol{D}_i$ as follows:

$$\phi_{xi} = (0,\ 0,\ 1)\boldsymbol{D}_i(0,\ 1,\ 0)^T \tag{2}$$

$$\phi_{yi} = (1,\ 0,\ 0)\boldsymbol{D}_i(0,\ 0,\ 1)^T \tag{3}$$

$$\phi_{zi} = (0,\ 1,\ 0)\boldsymbol{D}_i(1,\ 0,\ 0)^T \tag{4}$$

Substitution of Eq. (1) into Eqs. (2-4) yields

$$\phi_{xi} = \boldsymbol{t}_{c3}^T \boldsymbol{t}_{i2} \tag{5}$$

$$\phi_{yi} = \boldsymbol{t}_{c1}^T \boldsymbol{t}_{i3} \tag{6}$$

$$\phi_{zi} = \boldsymbol{t}_{c2}^T \boldsymbol{t}_{i1} \tag{7}$$

where $\boldsymbol{t}_{cj}$ and $\boldsymbol{t}_{ij}$ are the jth column of $\boldsymbol{T}_c$ and $\boldsymbol{T}_i$, respectively. Since the x axis of $\boldsymbol{T}_c$ lies on the line connecting nodes 1 and 2, the direction cosines of the vector from nodes 1 to 2, which is the first column of $\boldsymbol{T}_c$, can be written as

$$\boldsymbol{t}_{c1} = (\boldsymbol{r}_2 - \boldsymbol{r}_1 + \boldsymbol{r}_0)/L \tag{8}$$

where $\boldsymbol{r}_0$ is a vector from node 1 to node 2 in the initial configuration. The z_c axis of $\boldsymbol{T}_c$, the third column of $\boldsymbol{T}_c$, is the cross product of $\boldsymbol{t}_{c1}$ and $\boldsymbol{t}_{i2}$, namely,

$$\boldsymbol{t}_{c3} = \tilde{\boldsymbol{t}}_{c1} \boldsymbol{t}_{i2} \tag{9}$$

The Y_c axis can be obtained by taking the cross product of $\boldsymbol{t}_{c3}$ and $\boldsymbol{t}_{c1}$,

$$\boldsymbol{t}_{c2} = \tilde{\boldsymbol{t}}_{c3} \boldsymbol{t}_{c1} \tag{10}$$

where ~ denotes a skew-symmetric matrix, for example,

$$\tilde{\boldsymbol{a}} = \begin{bmatrix} 0 & -a_z & a_y \\ a_z & 0 & -a_x \\ -a_y & a_x & 0 \end{bmatrix}$$

where a_x, a_y, and a_z are the vector components of vector $\boldsymbol{a}$. Note that $\tilde{\boldsymbol{a}}^T = -\tilde{\boldsymbol{a}}$ and that $\tilde{\boldsymbol{a}}\boldsymbol{b} = -\tilde{\boldsymbol{b}}\boldsymbol{a}$, which agrees with the vector product property $\boldsymbol{a}\times\boldsymbol{b} = -\boldsymbol{b}\times\boldsymbol{a}$.

Let $\boldsymbol{\rho} = [x_c,\ y_c,\ z_c]$ be the position vector of an arbitrary point P in the beam element, defined with respect to $\boldsymbol{T}_c$.

The displacement of a point P on a beam element due to flexural deformation may be expressed as

$$\boldsymbol{u} = \boldsymbol{N}\boldsymbol{\Phi} \tag{11}$$

where $\boldsymbol{N}$ is a 3×6 matrix of shape functions similar to that used in the standard finite element method, i.e.,

$$\boldsymbol{N} = \begin{bmatrix} 0 & (1-4\xi+3\xi^2)L\zeta & (-1+4\xi-3\xi^2)L\eta & 0 & (-2\xi+3\xi^2)L\zeta & (2\xi-3\xi^2)L\eta \\ -(1-\xi)L\zeta & 0 & (\xi-2\xi^2+\xi^3)L & -L\xi\zeta & 0 & (-\xi^2+\xi^3)L \\ -(1-\xi)L\eta & (-\xi+2\xi^2-\xi^3)L & 0 & -L\xi\eta & (\xi^2-\xi^3)L & 0 \end{bmatrix}$$

Here, ξ, η, and ζ have been nondimensionalized with respect to the beam element length L, i.e., $\xi = x_c/L$, $\eta = y_c/L$, and $\zeta = z_c/L$. Also in Eq. (11), Φ is the composite vector of rotation angles of nodes 1 and 2, i.e.,

$$\Phi = [\phi_{x1},\ \phi_{y1},\ \phi_{z1},\ \phi_{x2},\ \phi_{y2},\ \phi_{z2}]^T$$

The total displacement of point P as shown in Fig. 1 is, in vector form,

$$r^P = r_1 + \rho + u - \rho_0$$

where ρ is the vector $[x_c,\ y_c,\ z_c]^T$, and in algebraic form,

$$r^P = r_1 + T_c\rho + T_c u - T_{co}\rho_o \tag{12}$$

where T_{co} is the initial transformation matrix of T_c, and ρ_o is the initial position vector of point P in T_c. Note that axial deformation is implicitly included in the second term of the right-hand side of Eq. (12).

Super Beam Element

In some multibody formulations, the joint connection between elements is imposed through constraint equations. Here, instead of introducing additional constraints, extra degrees of freedom are added to the original element, i.e., additional generalized coordinates are added and a super beam element consisting of joint and beam is formed.

A beam element with rigid joint bodies at both ends is shown in Fig. 2. For simplicity, assume that no other element is attached to either joint body and each joint has a single degree-of-freedom hinge. For each joint body, an $O_iX_iY_iZ_i$ $(i = 1,2)$ body reference frame is chosen to locate and orient the joint body in the inertia frame. Vectors R_i $(i = 1,2)$ from the origin of the initial body reference frame to the origin of the current body reference frame define the global displacement of joint bodies 1 and 2. Transformation matrices Γ_i from joint body reference frames to the global frame define orientations of the joint body. Vectors that locate joint attachment points in joint bodies are denoted s_i $(i = 1,2)$ and are defined with respect to joint body reference frames. Therefore, nodal displacements r_i of the beam element can be represented by the joint body displacements R_i as

$$r_i = R_i + \Gamma_i s_i - \Gamma_{io} s_i \tag{13}$$

To determine the relation between T_i and Γ_i, consider coordinate systems $o_iX_i'Y_i'Z_i'$ and $o_ix_i'y_i'z_i'$ that are located at a joint attachment point; one fixed to the joint body and one fixed to the nodal frame. Initially, let $o_iX_i'Y_i'Z_i'$ and $o_ix_i'y_i'z_i'$ coincide with the z axes parallel to the hinge axis. Then, the difference in orientations of both systems at any time is the relative rotation about the hinge axis. The transformation matrix from the $o_ix_i'y_i'z_i'$ system to $o_iX_i'Y_i'Z_i'$ system is

$$\Theta_i = \begin{bmatrix} \cos\theta_i & -\sin\theta_i & 0 \\ \sin\theta_i & \cos\theta_i & 0 \\ 0 & 0 & 1 \end{bmatrix}$$

where θ_i is the relative rotation angle. The transformation matrix from joint body frame to the nodal reference frame can be obtained by sequential transformations as

$$T_i = \Gamma_i \Gamma_i' \Theta_i T_i'^T \tag{14}$$

where Γ_i' and T_i' are the transformation matrices of the $o_iX_i'Y_i'Z_i'$ and $o_ix_i'y_i'z_i'$ systems with respect to the $O_iX_iY_iZ_i$ and $o_ix_iy_iz_i$ systems, respectively.

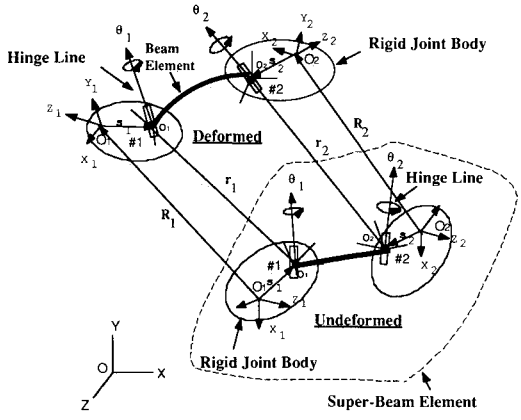

Fig. 2 Kinematics of super beam element.

Equations (13) and (14) may be substituted into Eq. (12) to obtain the displacement of an arbitrary point in the beam and can be represented in terms of displacements and orientations of joint bodies at the ends of the beam element, and relative rotations of joint degrees of freedom, i.e.,

$$r^P = G(R_1,\ \Gamma_1,\ \theta_1,\ R_2,\ \Gamma_2,\ \theta_2) \tag{15}$$

Variational Equations of Motion of a Super Beam Element

The variational equations of motion of a beam element at time t for a virtual displacement field that is consistent with the constraints is written as

$$-\int_\Omega \mu \delta r^{P^T} \ddot{r}^P \, d\Omega + \int_\Omega \delta r^{P^T} f^P \, d\Omega + \int_\sigma \delta r^{P^T} h^P \, d\sigma = \int_\Omega \delta\epsilon^{P^T} \tau^P \, d\Omega \tag{16}$$

where δr^P is a virtual displacement of point P that is consistent with constraints, $\ddot{r}^P$ the acceleration of point P, f^P the body force density at point P, h^P the surface traction at point P, $\delta\epsilon^P$ the kinematically compatible strain variation vector, τ^P the associated stress vector at point P, and Ω and σ the volume and surface of the beam before it is deformed.

By taking the variation of Eq. (15), the virtual displacement of point P is obtained as

$$\delta r^P = g_{R_1}\delta R_1 + g_{\Gamma_1}\delta\pi_1 + g_{\theta_1}\delta\theta_1 + g_{R_2}\delta R_2 + g_{\Gamma_2}\delta\pi_2 + g_{\theta_2}\delta\theta_2 \tag{17}$$

where $\delta\pi_i$ is the virtual rotation of Γ_i. Therefore, the virtual displacement of a point P in the beam element is represented by the virtual displacements and rotations of the joint bodies and virtual rotations of relative joint degrees of freedom.

The acceleration vector of a typical point can be obtained by taking two time derivatives of Eq. (15), which gives

$$\ddot{r}^P = g_{R_1}\ddot{R}_1 + g_{\Gamma_1}\dot{\omega}_1 + g_{\theta_1}\ddot{\theta}_1 + g_{R_2}\ddot{R}_2 + g_{\Gamma_2}\dot{\omega}_2 + g_{\theta_2}\ddot{\theta}_2 + \dot{g}_{R_1}\dot{R}_1 + \dot{g}_{\Gamma_1}\omega_1 + \dot{g}_{\theta_1}\dot{\theta}_1 + \dot{g}_{R_2}\dot{R}_2 + \dot{g}_{\Gamma_2}\omega_2 + \dot{g}_{\theta_2}\dot{\theta}_2 \tag{18}$$

where ω_i and $\dot{\omega}_i$ are angular velocity and angular acceleration of the joint body i.

Substituting Eqs. (17) and (18) into Eq. (16), the first term is

$$-\int_\Omega \mu \delta \boldsymbol{r}^{P^T} \ddot{\boldsymbol{r}}^P \, d\Omega = -\left[\delta \boldsymbol{R}_1^T,\ \delta \boldsymbol{\pi}_1^T,\ \delta\theta_1,\ \delta \boldsymbol{R}_2^T,\ \delta \boldsymbol{\pi}_2^T,\ \delta\theta_2\right]\left\{ \boldsymbol{M} \begin{bmatrix} \ddot{\boldsymbol{R}}_1 \\ \dot{\boldsymbol{\omega}}_1 \\ \ddot{\theta}_1 \\ \ddot{\boldsymbol{R}}_2 \\ \dot{\boldsymbol{\omega}}_2 \\ \ddot{\theta}_2 \end{bmatrix} + \boldsymbol{S}(\dot{\boldsymbol{R}}_1,\ \boldsymbol{\omega}_1,\ \dot{\theta}_1,\ \dot{\boldsymbol{R}}_2,\ \boldsymbol{\omega}_2,\ \dot{\theta}_2) \right\} \tag{19}$$

where $\boldsymbol{M}$ is the generalized mass matrix,

$$\boldsymbol{M} = \int_\Omega \mu \begin{bmatrix} \boldsymbol{g}_{R_1}^T\boldsymbol{g}_{R_1} & \boldsymbol{g}_{R_1}^T\boldsymbol{g}_{\Gamma_1} & \boldsymbol{g}_{R_1}^T\boldsymbol{g}_{\theta_1} & \boldsymbol{g}_{R_1}^T\boldsymbol{g}_{R_2} & \boldsymbol{g}_{R_1}^T\boldsymbol{g}_{\Gamma_2} & \boldsymbol{g}_{R_1}^T\boldsymbol{g}_{\theta_2} \\ & \boldsymbol{g}_{\Gamma_1}^T\boldsymbol{g}_{\Gamma_1} & \boldsymbol{g}_{\Gamma_1}^T\boldsymbol{g}_{\theta_1} & \boldsymbol{g}_{\Gamma_1}^T\boldsymbol{g}_{R_2} & \boldsymbol{g}_{\Gamma_1}^T\boldsymbol{g}_{\Gamma_2} & \boldsymbol{g}_{\Gamma_1}^T\boldsymbol{g}_{\theta_2} \\ & & \boldsymbol{g}_{\theta_1}^T\boldsymbol{g}_{\theta_1} & \boldsymbol{g}_{\theta_1}^T\boldsymbol{g}_{R_2} & \boldsymbol{g}_{\theta_1}^T\boldsymbol{g}_{\Gamma_2} & \boldsymbol{g}_{\theta_1}^T\boldsymbol{g}_{\theta_2} \\ & & & \boldsymbol{g}_{R_2}^T\boldsymbol{g}_{R_2} & \boldsymbol{g}_{R_2}^T\boldsymbol{g}_{\Gamma_2} & \boldsymbol{g}_{R_2}^T\boldsymbol{g}_{\theta_2} \\ & & & & \boldsymbol{g}_{\Gamma_2}^T\boldsymbol{g}_{\Gamma_2} & \boldsymbol{g}_{\Gamma_2}^T\boldsymbol{g}_{\theta_2} \\ \text{Symmetric} & & & & & \boldsymbol{g}_{\theta_2}^T\boldsymbol{g}_{\theta_2} \end{bmatrix} d\Omega$$

where the axial deformation

$$u_1 = \sqrt{(r_2 - r_1 + r_o)^T(r_2 - r_1 + r_o)} - \sqrt{r_o^T r_o}$$

and u_2 and u_3 are bending displacements in the y and z directions, respectively, of the neutral axis, which can be obtained from Eq. (11), and $\boldsymbol{U}$ is the generalized internal force vector.

Equations (19–21) may be substituted into Eq. (16), and the variational equation of motion of a super beam element then can be written as

$$\left[\delta \boldsymbol{R}_1^T,\ \delta \boldsymbol{\pi}_1^T,\ \delta\theta_1,\ \delta \boldsymbol{R}_2^T,\ \delta \boldsymbol{\pi}_2^T,\ \delta\theta_2\right]\left\{ \boldsymbol{M} \begin{bmatrix} \ddot{\boldsymbol{R}}_1 \\ \dot{\boldsymbol{\omega}}_1 \\ \ddot{\theta}_1 \\ \ddot{\boldsymbol{R}}_2 \\ \dot{\boldsymbol{\omega}}_2 \\ \ddot{\theta}_2 \end{bmatrix} + \boldsymbol{S}(\dot{\boldsymbol{R}}_1,\ \boldsymbol{\omega}_1,\ \dot{\theta}_1, \dot{\boldsymbol{R}}_2,\ \boldsymbol{\omega}_2,\ \dot{\theta}_2) + \boldsymbol{U} - \boldsymbol{Q} \right\} = 0 \tag{22}$$

and $\boldsymbol{S}$ is quadratic in velocity,

$$\boldsymbol{S} = \int_\Omega \mu \begin{bmatrix} \boldsymbol{g}_{R_1}^T(\dot{\boldsymbol{g}}_{R_1}\dot{\boldsymbol{R}}_1 + \dot{\boldsymbol{g}}_{\Gamma_1}\boldsymbol{\omega}_1 + \dot{\boldsymbol{g}}_{\theta_1}\dot{\theta}_1 + \dot{\boldsymbol{g}}_{R_2}\dot{\boldsymbol{R}}_2 + \dot{\boldsymbol{g}}_{\Gamma_2}\boldsymbol{\omega}_2 + \dot{\boldsymbol{g}}_{\theta_2}\dot{\theta}_2) \\ \boldsymbol{g}_{\Gamma_1}^T(\dot{\boldsymbol{g}}_{R_1}\dot{\boldsymbol{R}}_1 + \dot{\boldsymbol{g}}_{\Gamma_1}\boldsymbol{\omega}_1 + \dot{\boldsymbol{g}}_{\theta_1}\dot{\theta}_1 + \dot{\boldsymbol{g}}_{R_2}\dot{\boldsymbol{R}}_2 + \dot{\boldsymbol{g}}_{\Gamma_2}\boldsymbol{\omega}_2 + \dot{\boldsymbol{g}}_{\theta_2}\dot{\theta}_2) \\ \boldsymbol{g}_{\theta_1}^T(\dot{\boldsymbol{g}}_{R_1}\dot{\boldsymbol{R}}_1 + \dot{\boldsymbol{g}}_{\Gamma_1}\boldsymbol{\omega}_1 + \dot{\boldsymbol{g}}_{\theta_1}\dot{\theta}_1 + \dot{\boldsymbol{g}}_{R_2}\dot{\boldsymbol{R}}_2 + \dot{\boldsymbol{g}}_{\Gamma_2}\boldsymbol{\omega}_2 + \dot{\boldsymbol{g}}_{\theta_2}\dot{\theta}_2) \\ \boldsymbol{g}_{R_2}^T(\dot{\boldsymbol{g}}_{R_1}\dot{\boldsymbol{R}}_1 + \dot{\boldsymbol{g}}_{\Gamma_1}\boldsymbol{\omega}_1 + \dot{\boldsymbol{g}}_{\theta_1}\dot{\theta}_1 + \dot{\boldsymbol{g}}_{R_2}\dot{\boldsymbol{R}}_2 + \dot{\boldsymbol{g}}_{\Gamma_2}\boldsymbol{\omega}_2 + \dot{\boldsymbol{g}}_{\theta_2}\dot{\theta}_2) \\ \boldsymbol{g}_{\Gamma_2}^T(\dot{\boldsymbol{g}}_{R_1}\dot{\boldsymbol{R}}_1 + \dot{\boldsymbol{g}}_{\Gamma_1}\boldsymbol{\omega}_1 + \dot{\boldsymbol{g}}_{\theta_1}\dot{\theta}_1 + \dot{\boldsymbol{g}}_{R_2}\dot{\boldsymbol{R}}_2 + \dot{\boldsymbol{g}}_{\Gamma_2}\boldsymbol{\omega}_2 + \dot{\boldsymbol{g}}_{\theta_2}\dot{\theta}_2) \\ \boldsymbol{g}_{\theta_2}^T(\dot{\boldsymbol{g}}_{R_1}\dot{\boldsymbol{R}}_1 + \dot{\boldsymbol{g}}_{\Gamma_1}\boldsymbol{\omega}_1 + \dot{\boldsymbol{g}}_{\theta_1}\dot{\theta}_1 + \dot{\boldsymbol{g}}_{R_2}\dot{\boldsymbol{R}}_2 + \dot{\boldsymbol{g}}_{\Gamma_2}\boldsymbol{\omega}_2 + \dot{\boldsymbol{g}}_{\theta_2}\dot{\theta}_2) \end{bmatrix} d\Omega$$

Similarly, the second and third term in Eq. (16) become

$$\int_\Omega \delta \boldsymbol{r}^{P^T} \boldsymbol{f}^P \, d\Omega + \int_\sigma \delta \boldsymbol{r}^{P^T} \boldsymbol{h}^P \, d\sigma = \left[\delta \boldsymbol{R}_1^T,\ \delta \boldsymbol{\pi}_1^T,\ \delta\theta_1,\ \delta \boldsymbol{R}_2^T,\ \delta \boldsymbol{\pi}_2^T,\ \delta\theta_2\right]\boldsymbol{Q} \tag{20}$$

where $\boldsymbol{Q}$ is the external generalized force vector,

$$\boldsymbol{Q} = \int_\Omega \begin{bmatrix} \boldsymbol{g}_{R_1}^T\boldsymbol{f}^P \\ \boldsymbol{g}_{\Gamma_1}^T\boldsymbol{f}^P \\ \boldsymbol{g}_{\theta_1}^T\boldsymbol{f}^P \\ \boldsymbol{g}_{R_2}^T\boldsymbol{f}^P \\ \boldsymbol{g}_{\Gamma_2}^T\boldsymbol{f}^P \\ \boldsymbol{g}_{\theta_2}^T\boldsymbol{f}^P \end{bmatrix} d\Omega + \int_\sigma \begin{bmatrix} \boldsymbol{g}_{R_1}^T\boldsymbol{h}^P \\ \boldsymbol{g}_{\Gamma_1}^T\boldsymbol{h}^P \\ \boldsymbol{g}_{\theta_1}^T\boldsymbol{h}^P \\ \boldsymbol{g}_{R_2}^T\boldsymbol{h}^P \\ \boldsymbol{g}_{\Gamma_2}^T\boldsymbol{h}^P \\ \boldsymbol{g}_{\theta_2}^T\boldsymbol{h}^P \end{bmatrix} d\sigma$$

For a Bernoulli beam, the right-hand side of Eq. (16), which is the virtual work done by the internal force, may be expressed as

$$\int_\Omega \delta\boldsymbol{\epsilon}^{P^T}\boldsymbol{\tau}^P \, d\Omega = \int_0^L \left\{EAu_1\delta u_1 + EI_y u_2''\delta u_2'' + EI_z u_3''\delta u_3'' + GJ\phi_{x2}\delta\phi_{x2}\right\} dx_c = \left[\delta \boldsymbol{R}_1^T,\ \delta \boldsymbol{\pi}_1^T,\ \delta\theta_1,\ \delta \boldsymbol{R}_2^T,\ \delta \boldsymbol{\pi}_2^T,\ \delta\theta_2\right]\boldsymbol{U} \tag{21}$$

for all virtual displacements $\delta\boldsymbol{R}_1$ and $\delta\boldsymbol{R}_2$, virtual rotations $\delta\boldsymbol{\pi}_1$ and $\delta\boldsymbol{\pi}_2$, and virtual hinge rotations $\delta\theta_1$ and $\delta\theta_2$ that are consistent with the constraints.

Equations of Motion of the Constrained Systems

To form the equations of motion of a mechanical system that consists of n nodes and m hinges, the variational equations of motion of a generic element given in Eq. (22) are used to generate equations recursively for all of the elements in the system. For compatibility, the variational equations of motion of the system are assembled as is done in the standard finite element method. To treat the complete system, it is convenient to define a composite vector of variations of system variables $\delta\boldsymbol{q}$,

$$\delta\boldsymbol{q} = \left[\delta \boldsymbol{R}_1^T, \delta \boldsymbol{\pi}_1^T, \delta \boldsymbol{R}_2^T, \delta \boldsymbol{\pi}_2^T, \ \dots\ , \delta \boldsymbol{R}_n^T, \delta \boldsymbol{\pi}_n^T, \delta\theta_1, \delta\theta_2, \ \dots\ , \delta\theta_m\right]$$

and its associated acceleration vector $\ddot{\boldsymbol{q}}$,

$$\ddot{\boldsymbol{q}} = \left[\ddot{\boldsymbol{R}}_1^T, \dot{\boldsymbol{\omega}}_1^T, \ddot{\boldsymbol{R}}_2^T, \dot{\boldsymbol{\omega}}_2^T, \ \dots\ , \ddot{\boldsymbol{R}}_n^T, \dot{\boldsymbol{\omega}}_n^T, \ddot{\theta}_1, \ddot{\theta}_2, \ \dots\ , \ddot{\theta}_m\right]$$

The variational equations of motion of the system in this notation are assembled and written in the form

$$\delta\boldsymbol{q}^T\{\boldsymbol{M}^*\ddot{\boldsymbol{q}} - \boldsymbol{F}\} = 0 \tag{23}$$

which must hold for all $\delta\boldsymbol{q}$ that are consistent with constraints that act on the system, i.e.,

$$\boldsymbol{\Phi}_q \delta\boldsymbol{q} = 0 \tag{24}$$

In Eq. (23), $\boldsymbol{M}^*$ and $\boldsymbol{F}$ are the system mass matrix and generalized forces vector, respectively, and $\boldsymbol{\Phi}_q$ is the constraint Jacobian of the system.

Using Gaussian elimination, Eq. (24) can be put into Jordan canonical form

$$\left[\boldsymbol{I}\ ,\ \boldsymbol{\Phi}_{q_i}\right]\begin{bmatrix} \delta\boldsymbol{q}_d \\ \delta\boldsymbol{q}_i \end{bmatrix} = 0$$

or

$$\delta q_d = -\Phi_{qi}\delta q_i$$

where δq_d and δq_i are the variations of dependent and independent system variables, respectively. Therefore,

$$\delta q = \begin{bmatrix} \delta q_d \\ \delta q_i \end{bmatrix} = \begin{bmatrix} -\Phi_{qi} \\ I \end{bmatrix} \delta q_i = C\delta q_i \tag{25}$$

Acceleration equations of constraint are obtained by differentiating the constraint equations twice with respect to time to get

$$\Phi_q \ddot{q} = \gamma \tag{26}$$

where γ is the resulting right-hand side. Similarly, Eq. (26) can be decomposed into dependent and independent parts, which has the relation

$$\ddot{q}_d = -\Phi_{qi}\ddot{q}_i + \gamma \tag{27}$$

Therefore, the generalized acceleration vector is written as

$$\ddot{q} = \begin{bmatrix} \ddot{q}_d \\ \ddot{q}_i \end{bmatrix} = \begin{bmatrix} \gamma \\ 0 \end{bmatrix} + \begin{bmatrix} -\Phi_{qi} \\ I \end{bmatrix} \ddot{q}_i = R + C\ddot{q}_i \tag{28}$$

The substitution of Eqs. (25) and (28) into Eq. (23) yields

$$\delta q_i^T (C^T M^* C\ddot{q}_i + C^T M^* R - F) = 0 \tag{29a}$$

or

$$\delta q_i^T (M_s \ddot{q}_i - F_s) = 0 \tag{29b}$$

Since δq_i is arbitrary, Eqs. (29) are the equations of motion of the system in terms of independent system variables, i.e.,

$$M_s \ddot{q}_i - F_s = 0 \tag{30}$$

where $M_s = C^T M^* C$ is the equivalent system mass matrix, and $F_s = F - C^T M^* R$ is the equivalent generalized forces vector. After $\ddot{q}_i$ is found from Eq. (30), $\ddot{q}_d$ can be obtained from Eq. (27).

Applications

Analysis of a Deployable Space Structure

The deployable space structure shown in Fig. 3 is a 20-m-long triangular cross section, joint dominated truss structure, referred to as the Mini-Mast. The structure is used at NASA Langley as a ground test article for research in the development of techniques in structural dynamic characterization of large space structures and control of flexible structures. A total of 18 bays, each 1.12 m long, make up the 20-m length of the beam above the deployer mechanism. One bay of the truss beam consists of three longerons, three diagonal members, and a batten triangular truss whose cross section fits inside a 1.4-m-diam circle. The longerons and diagonal members are connected to batten triangles at each corner (three corner bodies are built into each corner of the batten triangle) by revolute joints.

The system is deployed/retracted two bays at a time. During deployement/retraction, the vertices of two batten triangles are held fixed in orientation while a third batten triangle, located between the two fixed ones, rotates about the longitudinal axis. Upward/downward forces are then applied to deploy/retract the system. Revolute joints in corner bodies at each apex of the triangular cross section of each bay and a nearly overcenter hinge in each diagonal member allow the beam truss to deploy/fold into a repeatable beam/stack, as shown in Fig. 3. At the final stage of deploying, midhinge of the diagonal member is locked up to ensure that the system becomes a structure. It is reopened as retraction starts. Since each two deploying bays are symmetric to the middle batten triangle, it is sufficient to analyze only one bay of the system.

The objective of the analysis is to determine flexible member loads during deployment of one bay of the truss beam. Because of the symmetric geometry of the system, corner bodies are constrained to move on a 1.4-m-diam cylinder during deployment. The longerons and diagonal members are deformed, due to kinematic constraints imposed at the joints, during deployment. Therefore, orientations of revolute joints of the longeron and diagonal member play an important role in the design of the truss beam. A set of properly designed revolutes will decrease deformations, hence decreasing the force required to deploy the truss beam. The system is designed such that it is not deformed in its fully retracted position. The retracted state thus serves as a good starting point to analyze the system response during deployment.

Since the mast is deployed quite slowly, this is a quasistatic case where inertial forces play a secondary role. Nevertheless, the analysis discussed herein and embodied in the LATDYN program is applicable.

LATDYN Model Description

The model can be simplified by taking the advantage of symmetric geometry of the triangular cross section of the system. The upper triangle is constrained to only move along the rotate about the longitudinal axis of the truss; the LATDYN model of one bay of Mini-Mast reduces to three flexible longerons, three flexible diagonal members, and two batten triangles that are modeled as rigid bodies, as shown in Fig. 4. The lower batten triangle, batten triangle A in Fig. 4, is grounded. The upper batten triangle, batten triangle B in Fig. 4, is driven up and down. The batten triangles are connected to the longerons and diagonal members with revolute joint at each corner, respectively. The geometry and material properties of the longeron and diagonal members are listed in Table 1. The initial configuration of the model is chosen with the system in its fully packaged position, as shown in Fig. 4. Locations and orientations of each revolute joints of longeron and diagonal members are listed in Tables 2 and 3, respectively.

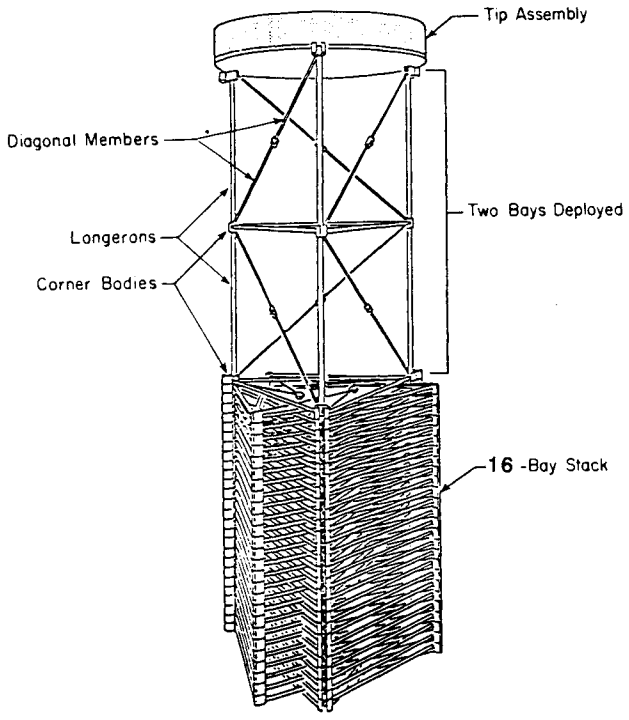

Fig. 3 Deployable space structure.

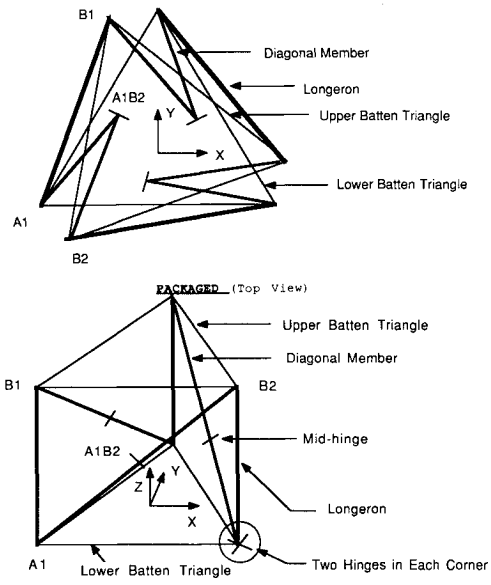

Fig. 4 One bay of Mini-Mast.

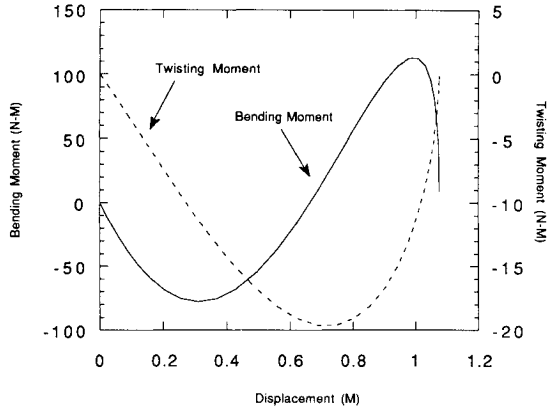

Fig. 5 Bending and twisting moment of the longeron at midpoint.

Results

The system is deployed by driving the upper triangle in the longitudinal direction without constraining its rotation about the longitudinal axis. The driving constraint is

$$Z = \frac{L}{T}\left[t - \frac{T}{2\pi}\sin\left(\frac{2\pi t}{T}\right)\right], \qquad t < T$$

$$Z = L, \qquad t \geq T$$

where L is the length of the longeron, T the total deploying time, and Z the height of the upper triangle. The deployment moves the upper triangle a distance L in the z direction in T seconds. In the simulations that follow, T is taken as 1.0 s.

Figure 5 shows the variations of the bending and twisting moments of the longeron at its midpoint, with the z displacement of the upper triangle. Figure 6 shows the bending moments of diagonal members A and B. Figure 7 shows the LATDYN results for the resultant bending moments of the longeron at the end joining the upper triangle. Also shown in the figure is the best result the authors can achieve using the assumed mode approach. To verify the results, consider a model that consists of the lower batten triangle and one of the longeron. Without the constraint of the upper batten triangle, the longeron can rotate about its joint freely and behaves like a rigid body. The trajectory of the tip end of the longeron projected on the x-y plane is shown in Fig. 8, along with the constrained trajectory (a section of the imaginary circle) if the upper batten triangle is modeled. Deviations of curves in Fig. 8 indicate the degree the longeron shall be bent to satisfy the kinematic constraints of the joints. It turns out that the two curves cross over as the longeron rotates about 50 deg. Therefore, the bending moment reaches its minimum value at this time step, which is exactly what the LATDYN prediction has shown in Fig. 7.

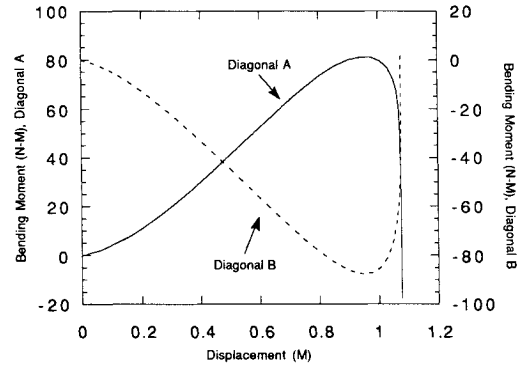

Fig. 6 Bending moment of diagonal A and B at midpoint.

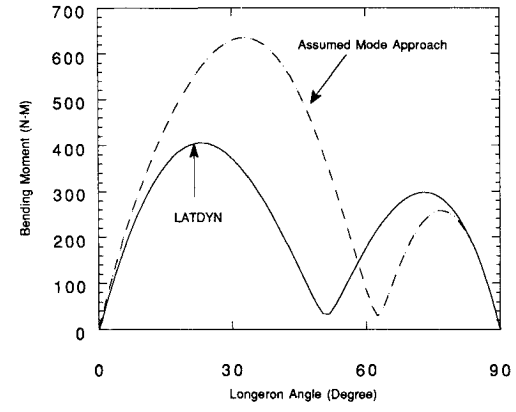

Fig. 7 Resultant bending moment of the longeron at upper end.

Table 1 Geometry and material properties

	Inner diameter, m	Outer diameter, m
Longeron	0.01491	0.02019
Diagonal member	0.01115	0.01511

Modulus of elasticity = 1.17E + 11 N/m^2
Shear modulus of elasticity = 4.0E + 9 N/m^2
Density = 1.616E + 3 kg/m^3

Table 2 Joint locations

Joint name	X	Y	Z
Longeron A1	−0.60598	−0.34987	0.02379
Longeron B1	−0.23372	0.65954	0.02379
Diagonal A1	−0.58031	−0.34987	0.02379
Diagonal B2	−0.49966	−0.50693	0.02379
Diagonal A1B2	−0.14861	0.26657	0.02379

Table 3 Joint orientations

Joint name	X component	Y component	Z component
Longeron A1	0.91838	0.07838	0.38786
Longeron B1	0.64757	−0.65591	−0.38786
Diagonal A1	0.98896	0.09973	−0.10956
Diagonal B2	0.88133	−0.39542	−0.25868
Diagonal A1B2	−0.88076	0.47339	0.01163

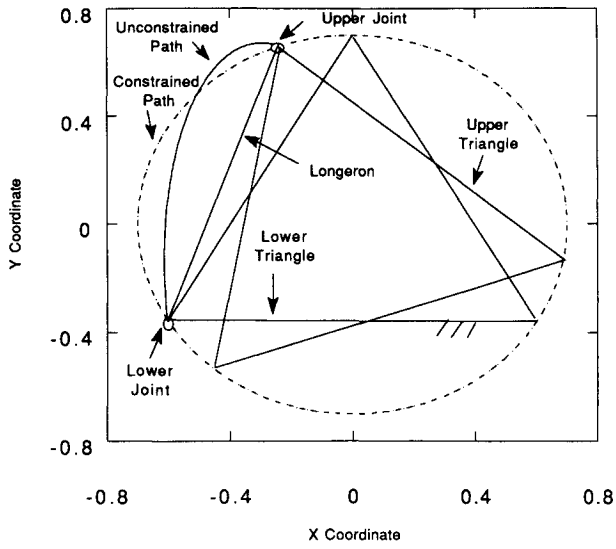

Fig. 8 Projected paths of constrained and unconstrained tip end of the longeron.

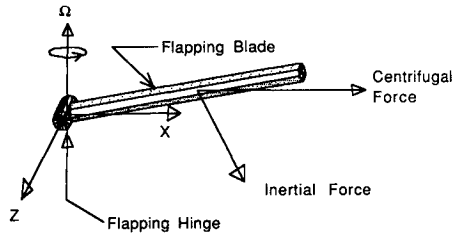

Fig. 9 Flapping blade.

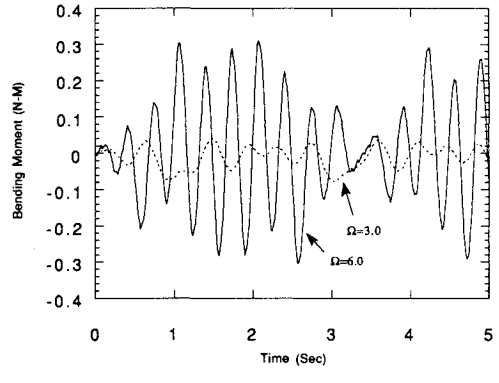

Fig. 10 Flapping bending moment: Ω = 3.0 and 6.0 rad/s.

Flapping Motion of Rotor Blade

System Description

A number of problems arise that make it necesssary to study the effects of the flexibility of a blade on its motion. For example, one may need to know whether the flexible motion affects the predicted performance, what stresses occur in the deformed blade, and whether the frequencies of the motion coincide with the natural frequencies of the flexible blade. An additional complicating factor is that, due to the stiffening effect of centrifugal forces, natural frequencies of the blade increase as blade rotational speed increases.

A simplified model of an articulated blade with no flap hinge offset of spring restraint is shown in Fig. 9. Initially, the blade is straight and tilted 0.157 rad. With no initial hinge velocity, the blade rotates at a constant speed. Since the centrifugal forces always act radially outward in a plane normal to the rotation axis, a force opposing the blade flap motion is induced.

Difficulties in modeling a rotating beam with the assumed mode approach have been reported in Refs. 5 and 6. In both cases, complete simulations are not achievable, due to diverging results. This is because the geometric stiffening effect is not properly accounted for[6,7] in the formulations using the assumed mode approach.

LATDYN Model and Results

In the simulation of the flapping blade using LATDYN, the rotational speed of the blade is kept constant in each simulation and gradually increased in succeeding simulations, starting with 1 rad/s and going up to 9 rad/s. Frequencies are calculated from the transient response of the simulation using a Fast Fourier Transform.

Figure 10 shows the bending moment in the blade at the midpoint at rotational speeds of 3 and 6 rad/s. The results clearly indicate that the natural frequency of the first flapping bending mode increases as the rotation speed increases, due to the centrifugal stiffening effect. Figure 11 displays natural frequencies of the first bending modes for different rotational speeds. For comparison, the solutions derived by Southwell[8] are also shown. Good agreement between the LATDYN results and the Southwell solutions is evident. Also shown (dotted lines) in Fig. 11 are different harmonics of the rotor speed. As shown, the natural frequency of the first mode intersects with the third harmonic around 8 rad/s, with the fourth harmonic at around 4 rad/s, the fifth harmonic around 3 rad/s, and so on for higher harmonics. It is known that resonances may occur when the blade rotation speed is near values around these speeds. Figure 12 shows the bending moment of the blade

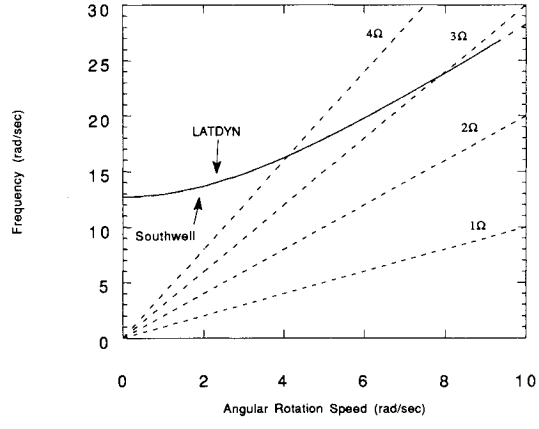

Fig. 11 Coalescence of flexible and rigid-body harmonics.

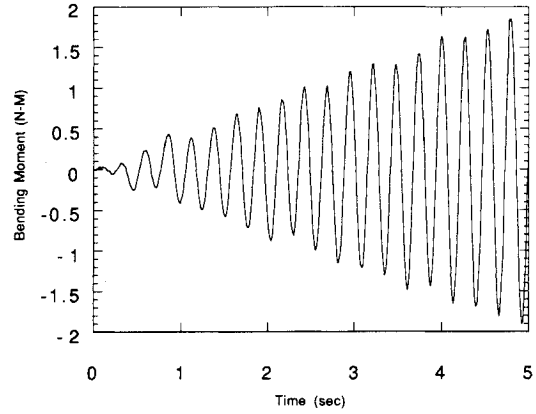

Fig. 12 Resonance of flapping blade: Ω = 8.0 rad/s.

when it rotates at 8 rad/s, which indicates that the magnitude of the bending blade keeps increasing the time. The magnitude of the response in Fig. 12 may increase indefinitely if the frequency of the blade is precisely three times of the rotational speed of the blade. In the case where the ratio between the natural frequency and rotational speed of the blade is not exactly 3, a phenomenon known as beating[9] may be observed in Fig. 12. For the blade under study, the frequency of the blade is exactly three times of the rotation speed of the blade when the blade is rotating at 7.87 rad/s. Therefore, the response shown in Fig. 12 is part of a beat with a long period.

Conclusions

A three-dimensional, finite element based simulation tool for flexible multibody systems has been described. Hinge degrees of freedom are built into the equations of motion to reduce geometry constraints. The approach avoids the difficulty in selecting deformation modes for flexible components by using the assumed mode method. Two applications of the program were discussed. For the first example, the program was used to simulate a practical space structure deployment problem. In the second example, the flapping motion of a rotating blade was simulated. Results for these two examples demonstrate the capabilties of the simulation code and the modeling aspects of the approach.

References

[1]Yoo, W. S., and Haug, E. J., "Dynamics of Articulated Structures, Part I: Theory and Part II: Computer Implementation and Applications," *Journal of Structure Mechanics,* Vol. 14, 1986, pp. 105–126, 177–189.

[2]Bodley, C. S., Devers, A. D., Park, A. C., and Frisch, H. P., "A Digital Computer Program for the Dynamic Interaction Simulation of Controls and Structure (DISCOS)," Vols. 1 & 2, NASA TP 1219, May 1978.

[3]Singh, R. P., VanderVoort, R. J., and Likins, P. W., "Dynamics of Flexible Bodies in Tree Topology—A Computer Oriented Approach," AIAA/ASME/ASCE 25th Structural Dynamics and Materials Conference, AIAA Paper 84-1024, Palm Springs, CA, May 1984.

[4]Goldstein, H., *Classical Mechanics,* 2nd ed., Addison-Wesley, Reading, MA, 1980.

[5]Wu, S. C., "A Substructure Method of Dynamic Simulation of Flexible Mechanical Systems with Geometric Nonlinearities," Ph.D. Dissertation, Univ. of Iowa, Iowa City, IA, May 1987.

[6]Kane, T. R., Ryan, R. R., and Banerjee, A. K., "Dynamics of A Beam Attached to a Moving Base," *Journal of Guidance, Control, and Dynamics,* Vol. 10, No. 2, 1987, pp. 139–151.

[7]McGowan, P. E., and Housner, J. M., "Nonlinear Dynamic Analysis of Deploying Flexible Space Booms," NASA TM-87617, Sept. 1985.

[8]Bramwell, A. R. S., *Helicopter Dynamics,* Wiley, New York, 1976, Chap. 9, p. 308.

[9]Timoshenko, S. P., Young, D. H., and Weaver, W., Jr., *Vibration Problems in Engineering,* 4th ed., Wiley, New York, 1974, Chap. 1, p. 62.